HEALTH AND MEDICINE

An engineering-reinforced extracellular vesicle–integrated hydrogel with an ROS-responsive release pattern mitigates spinal cord injury

Jian Cao[1]†, Xunqi Zhang[1]†, Jing Guo[1]†, Jiahe Wu[1], Lingmin Lin[2], Xurong Lin[2], Jiafu Mu[1], Tianchen Huang[3], Manning Zhu[1], Lan Ma[1], Weihang Zhou[1], Xinchi Jiang[1], Xuhua Wang[2], Shiqing Feng[4], Zhen Gu[1,5]*, Jian-Qing Gao[1,3,5,6,7]*

The local delivery of mesenchymal stem cell–derived extracellular vesicles (EVs) via hydrogel has emerged as an effective approach for spinal cord injury (SCI) treatment. However, achieving on-demand release of EVs from hydrogel to address dynamically changing pathology remains challenging. Here, we used a series of engineering methods to further enhance EVs' efficacy and optimize their release pattern from hydrogel. Specifically, the pro-angiogenic, neurotrophic, and anti-inflammatory effects of EVs were reinforced through three-dimensional culture and dexamethasone (Dxm) encapsulation. Then, the prepared Dxm-loaded 3EVs (3EVs-Dxm) were membrane modified with ortho-dihydroxy groups (-2OH) and formed an EV-integrated hydrogel (3EVs-Dxm-Gel) via the cross-link with phenylboronic acid–modified hyaluronic acid and tannic acid. The phenylboronic acid ester in 3EVs-Dxm-Gel enabled effective immobilization and reactive oxygen species–responsive release of EVs. Topical injection of 3EVs-Dxm-Gel in SCI rats notably mitigated injury severity and promoted functional recovery, which may offer opportunities for EV-based therapeutics in central nervous system injury.

INTRODUCTION

Spinal cord injury (SCI) seriously disrupts central nervous conduction, leading to motor and sensory dysfunction and even death, along with a series of physiological and psychological complications (*1*). Each year, there are at least 250,000 new cases of SCI worldwide (*2*). Although the survival rate of SCI patients has steadily improved in recent decades (*3*), the associated health burden and economic costs continue to rise, presenting a big challenge in clinic (*4*).

The pathology of SCI is extremely complicated. The initial trauma to the spinal cord causes tissue necrosis, hemorrhage, and edema, which in turn trigger secondary injury. Massive infiltration of inflammatory cells, including microglia, macrophages, and neutrophils, occurs at the lesion site, where they secrete pro-inflammatory cytokines such as tumor necrosis factor (TNF) and interleukin-1β (IL-1β). The impaired mitochondrial respiratory chain, combined with the activation of inflammatory cells, leads to excessive production of reactive oxygen species (ROS), causing peroxidation damage. In a word, the secondary injury exacerbates the injury degree and extends the injury area (*5*, *6*). Insufficient suppression of the secondary injury in the acute phase can lead to cystic cavities and glial scars, severely hindering tissue regeneration and functional recovery (*7*, *8*). Although the systemic administration of high-dose methylprednisolone was initially thought to be effective, the severe side effects have led to its discontinuation as a routine treatment (*9*). Hence, it is urgent to explore more strategies to mitigate severe SCI.

Fortunately, mesenchymal stem cell (MSC)–derived extracellular vesicles (EVs) were found to have abilities to alleviate neuroinflammation, inhibit neuronal apoptosis, and promote neurogenesis and differentiation (*10*, *11*). The secreted EVs with their cargos are ultimately taken up by target cells to exert regulatory effects, playing a crucial role in maintaining homeostasis (*12*). The aforementioned therapeutic activities make EVs highly suitable for treating the complicated pathology of SCI. Furthermore, with the advance of engineering technologies, the therapeutic efficacy of EVs can be reinforced for rapidly mitigating the severe condition of SCI, especially in the acute phase (*13*). However, the secondary injury process is dynamically changing and persists for several weeks (*14*). Chen *et al.* found that neutrophils, astrocytes, and microglial cells were activated at distinct time points in the first 3 days of SCI, contributing to the progressive inflammatory response. They proposed that anti-inflammatory intervention before day 3 may prevent the downstream adverse outcomes (*15*). Our previous research found that neuroinflammation in SCI rats peaked on day 4 and then gradually subsided within 7 days (*16*). Hence, on-demand regulation of SCI via EVs is urgently needed.

To this end, MSCs were cultured into three-dimensional (3D) MSC spheroid (MS) to extract its EVs (3EVs), which exhibited enhanced pro-angiogenic and neurotrophic effects than 2D MSC–derived EVs (2EVs). Dexamethasone (Dxm) was encapsulated in 3EVs via probe sonication to promote anti-inflammatory effect of 3EVs. The sonication energy was optimized to ensure that Dxm-loaded 3EVs (3EVs-Dxm) retained adequate drug content while maintaining structural integrity. For local delivery, 3EVs-Dxm were incubated with distearoyl phosphatidyl ethanolamine-polyethylene glycol$_{5000}$-propanediol (DSPE-PEG$_{5000}$-2OH) to modify with ortho-dihydroxy groups (-2OH). This

[1]State Key Laboratory of Advanced Drug Delivery and Release Systems, College of Pharmaceutical Sciences, Zhejiang University, Hangzhou 310058, China. [2]Department of Rehabilitation Medicine of First Affiliated Hospital and School of Brain Science and Brain Medicine, Zhejiang University School of Medicine, Hangzhou 310003, China. [3]Hangzhou Institute of Innovative Medicine, College of Pharmaceutical Sciences, Zhejiang University, Hangzhou 310058, China. [4]International Science and Technology Cooperation Base of Spinal Cord Injury, Tianjin Key Laboratory of Spine and Spinal Cord Injury, Department of Orthopedics, Tianjin Medical University General Hospital, Tianjin 300052, China. [5]Jinhua Institute of Zhejiang University, Jinhua 321002, China. [6]Dr. Li Dak Sum & Yip Yio Chin Center for Stem Cell and Regenerative Medicine, Zhejiang University, Hangzhou 310058, China. [7]Department of Pharmacy, The Second Affiliated Hospital, Zhejiang University School of Medicine, Hangzhou 310009, China.
*Corresponding author. Email: guzhen@zju.edu.cn (Z.G.); gaojianqing@zju.edu.cn (J.-Q.G.)
†These authors contributed equally to this work.

modification enabled 3EVs-Dxm to cross-link with phenylboronic acid–modified hyaluronic acid (HA-PBA) and tannic acid (TA), forming an injectable hydrogel termed 3EVs-Dxm-Gel (Fig. 1A). The formation of the PBA ester by -2OH and PBA in 3EVs-Dxm-Gel allowed for effective immobilization and ROS-responsive release of 3EVs-Dxm. This approach improved the therapeutic effects of EVs and their release pattern from hydrogel. Topical injection of 3EVs-Dxm-Gel into SCI rats was proposed as an effective strategy to alleviate oxidative damage and inflammation, creating a conducive microenvironment for neural repair and angiogenesis (Fig. 1B). This strategy aimed to address the complex pathology of SCI and promote functional recovery.

RESULTS

Extraction and characterization of 3EVs

To enhance the therapeutic effects of EVs, we added ascorbic acid in the culture medium of MSCs to facilitate the spontaneous formation of MS. The scanning electron microscopy (SEM) image showed that MS was ellipsoidal, with a long diameter of ~1.8 mm and a short diameter of ~1.3 mm (Fig. 2A). The surface of MS displayed a dense arrangement of MSCs with an extracellular matrix between the cells (Fig. 2B). MS was able to maintain a stable spheroid shape for more than 1 month, with the culture medium replaced every 3 days. The collected culture medium was stored at −80°C for EV extraction via the ultracentrifugation method.

Western blotting (WB) results proved that both 2EVs and 3EVs expressed biomarkers including CD9, CD63, and TSG101 (Fig. 2C). Transmission electron microscopy (TEM) images demonstrated that 2EVs and 3EVs had the typical cup-shaped morphology with comparable particle sizes (Fig. 2D). The data measured by a nanoparticle analyzer confirmed that 2EVs and 3EVs had similar particle sizes and zeta potentials, with sizes of ~138 and 135 nm and zeta potentials of −7.03 and −7.23 mV, respectively (fig. S1). These findings collectively proved the successful extraction of EVs.

Preparation of 3EVs-Dxm via the probe sonication method

To further enhance the anti-inflammatory effect of 3EVs, we encapsulated the clinically used drug Dxm into 3EVs via the probe sonication method within different sonication energies (0 to 15%). The drug content and encapsulation efficiency were measured using high-performance liquid chromatography (HPLC). When the sonication energy was 0%, 50 μg of 3EVs encapsulated 41.4 μg of Dxm, which

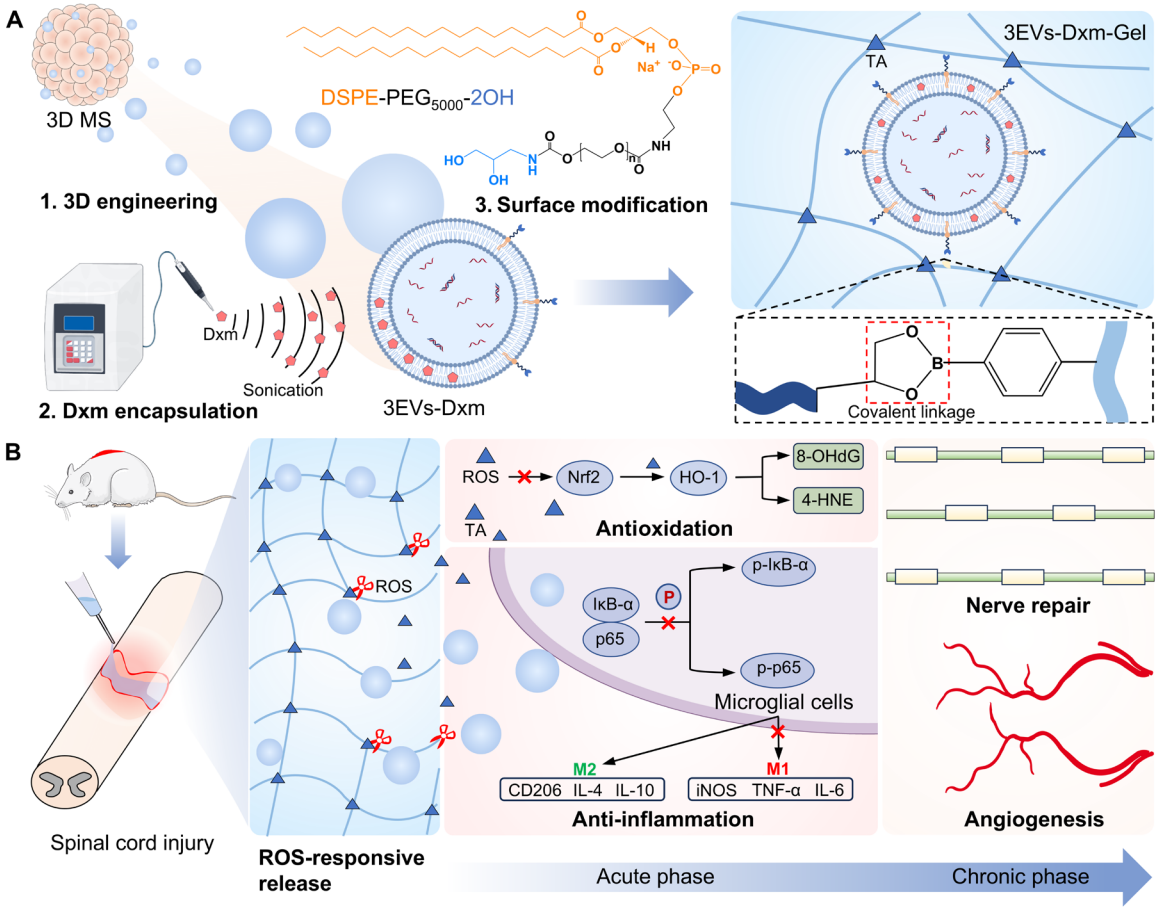

Fig. 1. Illustration of the stepwise preparation of 3EVs-Dxm-Gel and its proposed therapeutic mechanism in SCI treatment. (**A**) 3EVs extracted from MS were loaded with Dxm using the probe sonication method to obtain 3EVs-Dxm. Subsequently, 3EVs-Dxm were modified with -2OH groups and cross-linked with HA-PBA and TA to form an injectable hydrogel (3EVs-Dxm-Gel). (**B**) 3EVs-Dxm-Gel with an antioxidative effect was injected into the injured spinal cord and released anti-inflammatory 3EVs-Dxm in an ROS-responsive pattern. 3EVs-Dxm-Gel treatment attenuated oxidative damage and neuroinflammation during the acute phase, while it improved neural repair and angiogenesis in the chronic phase, thereby aiding in the function restoration following SCI.

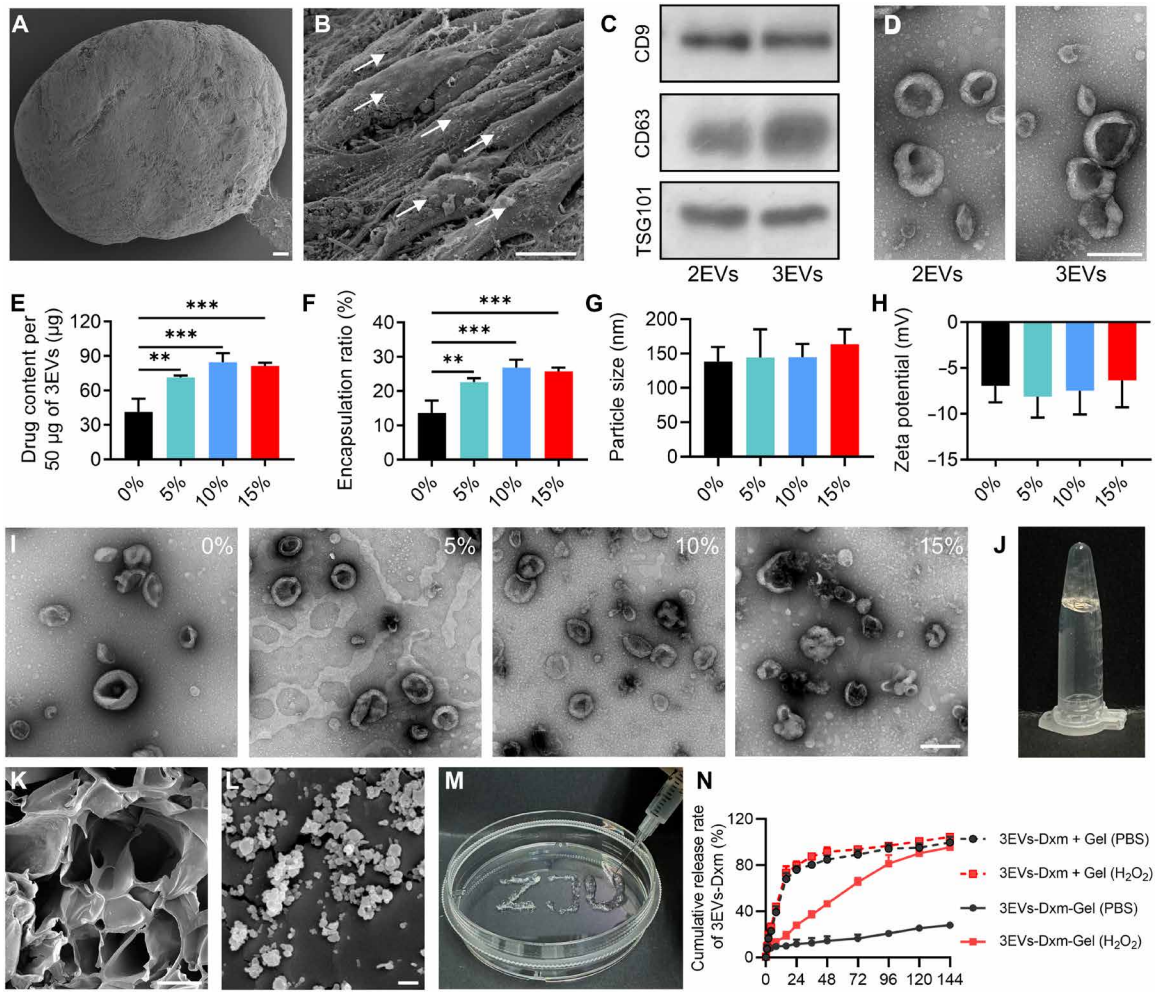

Fig. 2. Preparation and characterization of 3EVs-Dxm-Gel. (**A**) SEM images of MS (scale bar, 100 μm) and (**B**) its surface MSCs (scale bar, 10 μm). The white arrows indicate MSCs. (**C**) Expression of biomarkers of 2EVs and 3EVs including CD9, CD63, and TSG101. (**D**) TEM images of 2EVs and 3EVs. Scale bar, 200 nm. (**E**) Drug contents, (**F**) encapsulation ratios, (**G**) particle sizes, (**H**) zeta potentials, and (**I**) TEM images (scale bar, 200 nm) of 3EVs-Dxm fabricated with different sonication energies [(E) to (H) $n = 3$]. (**J**) Morphology, (**K**) inner structure, and (**L**) 3EVs-Dxm distribution of 3EVs-Dxm-Gel [scale bars, 50 μm (K) and 200 nm (L)]. (**M**) Injectable property of 3EVs-Dxm-Gel. (**N**) Cumulative release curve of EVs from 3EVs-Dxm-Gel and 3EVs-Dxm + Gel in PBS or H_2O_2 solutions ($n = 3$). $^{**}P < 0.01$ and $^{***}P < 0.001$.

was probably loaded through hydrophobic interactions between Dxm and the EV membrane during the co-incubation process. The addition of sonication considerably improved the drug content, especially with 10 and 15% sonication energies, which achieved 84.61 and 81.47μg of Dxm loading per 50 μg of 3EVs, respectively (Fig. 2E). The encapsulation efficiency was also improved from 13.58% with 0% sonication energy to 26.8% with 10% energy and 25.71% with 15% energy (Fig. 2F). Meanwhile, the particle size and zeta potential measurements showed no obvious changes in 3EVs with different sonication energies (Fig. 2, G and H). Nevertheless, TEM images revealed that the structure of 3EVs-Dxm prepared with 15% sonication energy was partially disrupted (Fig. 2I). Considering that 10% sonication energy greatly promoted Dxm loading and maintained the intact structure of 3EVs, it was used for the preparation of 3EVs-Dxm.

Construction of 3EVs-Dxm-Gel and its release pattern

For EV delivery, -2OH was modified on the membrane of 3EVs-Dxm, allowing 3EVs-Dxm to form PBA ester with HA-PBA. First, DSPE-PEG_{5000}-2OH was synthesized on the basis of the reaction between -NHS and -NH_2. The structure was confirmed by ^{1}H nuclear magnetic resonance (fig. S2). As a synthetic phospholipid, DSPE could be embedded into the phospholipid bilayer through hydrophobic interactions. During this process, the grafted -2OH was also modified on EVs' membrane. To measure the modification ratio, fluorescent DSPE-PEG_{5000}-Cy5 was used instead of DSPE-PEG_{5000}-2OH to prepare modified EVs and detected by Flow NanoAnalyzer. The data suggested that co-incubation at 37°C for 30 and 60 min could efficiently modify 3EVs-Dxm, reaching 86.2 and 89.9% of modification ratios, respectively (fig. S3). Then, the modified 3EVs-Dxm were grafted on synthesized HA-PBA (fig. S4) on the basis of the reaction between PBA and -2OH. Last, the remaining PBA on HA-PBA cross-linked with polyphenolic hydroxyl groups on TA to form an EV-integrated hydrogel, 3EVs-Dxm-Gel (Fig. 2J). SEM images showed a porous network structure of 3EVs-Dxm-Gel, with pore diameters ranging from 50 to 100 μm (Fig. 2K). A considerable amount of 3EVs-Dxm was distributed in the interior of the pores

(Fig. 2L). The injectability ensured that the hydrogel could be implanted in a minimally invasive manner and conformed to the size and shape of the lesion (Fig. 2M) (*17*). Rheological results indicated that 3EVs-Dxm-Gel exhibited similar mechanical characteristics to those of natural spinal cord (0.1 to 16 kPa) (*18*), making it suitable for local implantation (fig. S5).

ROS is a key factor in secondary injury and reflects the severity of SCI. PBA ester in 3EVs-Dxm-Gel is sensitive to ROS, which enables the release of encapsulated 3EVs-Dxm in response to ROS (*19*). To verify it, 3EVs-Dxm-Gel was placed in phosphate-buffered saline (PBS) solution. Only a small amount of 3EVs-Dxm was released in the initial stage, and 27.85% of EVs were released within 6 days. When placed in hydrogen peroxide (H_2O_2) solution, the cleavage of the PBA ester in 3EVs-Dxm-Gel resulted in a responsive release of 3EVs-Dxm until complete release on day 6 (Fig. 2N). As a control, the unmodified 3EVs-Dxm were mixed with HA-PBA and TA to form a gel termed 3EVs-Dxm + Gel. In the release test, regardless of PBS or H_2O_2 solution, ~80% of the unmodified 3EVs-Dxm were rapidly released from 3EVs-Dxm + Gel within 24 hours (Fig. 2N). This indicated that the covalent linkage between -2OH of modified 3EVs-Dxm and PBA of HA-PBA was the key to the ROS-responsive release pattern. In addition, the cleavage of the PBA ester also induced ROS-responsive degradation of 3EVs-Dxm-Gel and 3EVs-Dxm + Gel (fig. S6).

3EVs exhibited enhanced pro-angiogenic and neurotrophic capacities

Following the construction of 3EVs-Dxm-Gel, the therapeutic effects of 3EVs, 3EVs-Dxm, and 3EVs-Dxm-Gel were successively evaluated. First, the tissue repair and regeneration capacities of 3EVs were tested. Previous studies reported that MSC-derived EVs have certain effects on promoting angiogenesis and neurotrophic support, which are urgently needed for a good prognosis of SCI (*20*, *21*). The 3D culture used in this study would change the cargo content of EVs (*22*). Hence, to compare the differences between 2EVs and 3EVs in terms of pro-angiogenesis and neurotrophic effects, human umbilical vein endothelial cell (HUVEC) migration, tube formation, and PC12 cell differentiation experiments were conducted.

After incubation, HUVEC scratch in the 3EVs group was already visibly reduced compared with the control (Ctrl) group at 5 hours (fig. S7) and almost disappeared within 10 hours, showing better performance than the 2EVs group (Fig. 3, A and C). Moreover, after incubation with 2EVs or 3EVs for 4 hours, HUVECs gradually formed tube structures, while the untreated HUVECs only exhibited fewer complete tubular structures. In particular, the tube structures of HUVECs in the 3EVs group were more complete (Fig. 3B). Semi-quantitative analysis revealed that 3EVs significantly promoted tube formation compared to 2EVs, resulting in longer total branching length (Fig. 3D).

PC12 cells are known to differentiate and extend axons under the stimulation of nerve growth factor (NGF). Therefore, NGF was added to the culture medium to induce PC12 cell differentiation and outgrowth of axon structure. Both 2EVs and 3EVs were found to enhance cell differentiation (Fig. 3E), including higher differentiation rate, more axon counts per cell, and longer axon length. Also, 3EVs showed the best neurotrophic effects, especially in promoting axon length (Fig. 3, F to H). In summary, 3EVs had superiority over 2EVs in terms of pro-angiogenesis and neurotrophic support capabilities.

3EVs-Dxm demonstrated strong anti-inflammatory effects

The anti-inflammatory activity of Dxm relies on its intracellular binding to glucocorticoid receptors (*23*). Therefore, the cellular uptake of 3EVs-Dxm is crucial for its anti-inflammatory function. 3EVs-Dxm were labeled using 1,1′-dioctadecyl-3,3,3′,3′-tetramethylindocarbocyanine perchlorate (DiI), and the uptake by BV2 cells, HUVECs, and PC12 cells was assessed by flow cytometry. The results presented that 3EVs-Dxm were rapidly taken up by all three cell types within 60 min (fig. S8A). Meanwhile, BV2 cells, which were stimulated with lipopolysaccharide (LPS) to mimic activated microglial cells following SCI, had a strong phagocytic ability (*14*). The activated BV2 cells massively took up 3EVs-Dxm within 60 min, which posed a much higher cell uptake ratio and content than PC12 cells and HUVECs (fig. S8B). Given that microglial cells are key players in neuroinflammation (*24*), the rapid uptake of 3EVs-Dxm by microglial cells was beneficial for exerting their anti-inflammatory effects.

Furthermore, the anti-inflammatory effect of 3EVs-Dxm was evaluated in LPS-activated BV2 cells by detecting M1/M2 polarization and cytokine secretion. Immunofluorescence results showed that LPS-activated BV2 cells highly expressed an M1-related marker, inducible nitric oxide synthase (iNOS), indicating their tendency to the pro-inflammatory M1 type. iNOS expression slightly decreased after the administration of 3EVs, suggesting that 3EVs inherently have some anti-inflammatory activities, which is consistent with previous reports (*25*, *26*). Dxm is a potent anti-inflammatory drug that notably reduces the iNOS level in BV2 cells. Consequently, the combination of Dxm with 3EVs in 3EVs-Dxm greatly enhanced the anti-inflammatory capacity, bringing the iNOS level close to the normal level (Fig. 3I). The CD206 results indicated that only Dxm and 3EVs-Dxm distinctly promoted the M2 polarization in BV2 cells (Fig. 3J). The concentrations of M1-associated cytokines (TNF-α and IL-6) and M2-associated cytokines (IL-4 and IL-10) confirmed that 3EVs-Dxm obviously suppressed the release of pro-inflammatory factors and slightly increased the secretion of anti-inflammatory factors (Fig. 3K). In addition, when comparing the individual efficacy of 3EVs and Dxm, it was suggested that the strong anti-inflammatory activity of 3EVs-Dxm was mainly attributed to the encapsulated Dxm.

3EVs-Dxm-Gel posed an antioxidative effect

The polyphenolic hydroxyl of TA in 3EVs-Dxm-Gel can act as a hydrogen donor and thus is capable of neutralizing free radicals (*27*). PBA esters also have reducibility (*28*). Therefore, 3EVs-Dxm-Gel exhibited strong antioxidative capabilities. TA and 3EVs-Dxm-Gel were found to rapidly clean 2,2-diphenyl-1-picrylhydrazyl (DPPH), turning the solutions from purple to yellow and substantially reducing their optical density value at 490 nm (fig. S9A). Moreover, 3EVs-Dxm-Gel significantly suppressed the ROS levels in H_2O_2-stimulated PC12 cells (fig. S9, B and C). These data demonstrated the hydrogel's ability to mitigate oxidative stress, which is crucial for alleviating oxidative damage in SCI.

3EVs-Dxm-Gel alleviated the secondary injury of SCI rats

The SCI rat model was established by cutting off the spinal cord. 3EVs-Dxm and 3EVs-Dxm-Gel were injected into the lesion, and the in vivo fate of EVs on days 1, 4, and 7 was observed using a live imaging system. Because of the flushing of cerebrospinal fluid and blood in the spinal cord, the fluorescence signal of DiI-labeled EVs in the 3EVs-Dxm group rapidly declined on day 1 and had a brief retention time in the spinal cord. In contrast, EVs in 3EVs-Dxm-Gel were gradually released from the implantation site to the adjacent area and

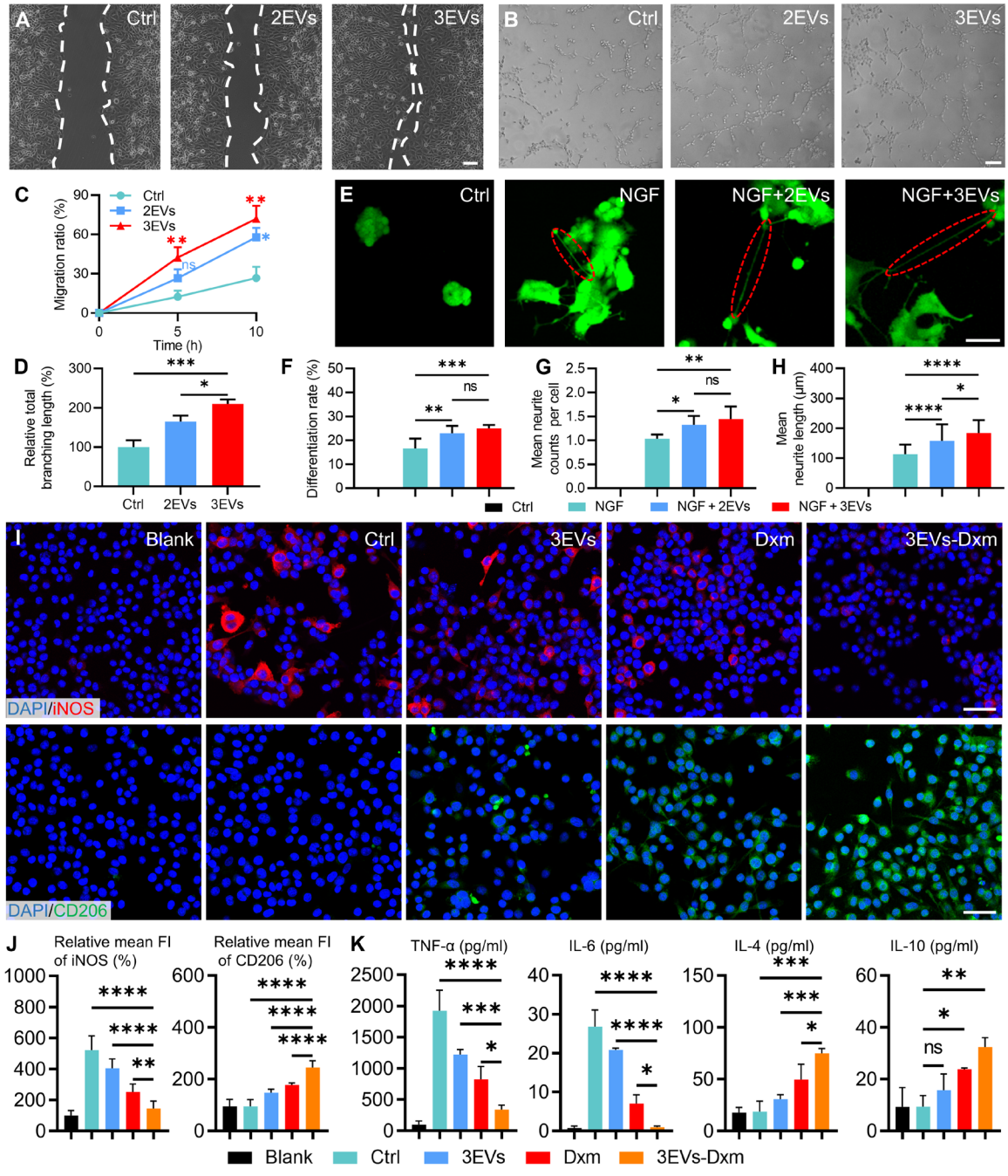

Fig. 3. Assessment of the therapeutic effects of 3EVs-Dxm. (**A**) HUVEC migration after 10 hours (scale bar, 100 μm) and (**B**) tube formation after 4 hours (scale bar, 100 μm) in the Ctrl, 2EVs, and 3EVs groups. (**C**) Semiquantitative analysis of cell migration within 10 hours ($n = 3$) and (**D**) total branching length of the tube ($n = 3$). (**E**) PC12 cell differentiation in Ctrl, NGF, NGF + 2EVs, and NGF + 3EVs groups (scale bar, 50 μm). The red oval indicates representative neurite (scale bar, 100 μm). (**F** to **H**) Semiquantitative analysis of differentiation rate (F) ($n = 3$; two regions per well were selected for statistical analysis), mean neurite counts per cell (G) ($n = 3$; two regions per well were selected for statistical analysis), and mean neurite length for PC12 cells with different treatments (H) ($n = 3$; 12 differentiated cells per well were selected for statistical analysis). The significance test of difference was conducted in NGF, NGF + 2EVs, and NGF + 3EVs groups. (**I**) iNOS and CD206 expressions of LPS-stimulated BV2 cells treated with 3EVs, Dxm, and 3EVs-Dxm and (**J**) their relative mean fluorescence intensity (FI) analysis (scale bars, 50 μm; $n = 3$). (**K**) TNF-α, IL-6, IL-4, and IL-10 secretions of LPS-stimulated BV2 cells with the treatments of 3EVs, Dxm, and 3EVs-Dxm ($n = 3$). $^{ns}P > 0.05$, $^{*}P < 0.05$, $^{**}P < 0.01$, $^{***}P < 0.001$, and $^{****}P < 0.0001$.

could still be detected on day 7, indicating the localized delivery capacity of 3EVs-Dxm-Gel (Fig. 4A and fig. S10A). Such a delivery approach facilitated the EVs' regulation of SCI over 1 week.

On day 4, a lipid peroxidation product, 4-hydroxynonenal (4-HNE), and a DNA peroxidation product, 8-hydroxy-2′-deoxyguanosine (8-OHdG), were detected in the spinal cord tissue of rats in each group. SCI markedly increased 4-HNE and 8-OHdG levels, suggesting severe oxidative damage to the spinal cord (Fig. 4B). The administration of 3EVs-Dxm and 3EVs-Dxm-Gel effectively inhibited the formation of peroxidation products. Owing to its longer in vivo retention time, 3EVs-Dxm-Gel had a better antioxidative effect than 3EVs-Dxm (fig. S10, B and C).

Simultaneously, 3EVs-Dxm and 3EVs-Dxm-Gel exhibited anti-inflammatory effects in the acute phase. On day 4, CD68-positive microglial cells could be detected in the lesion area in all rats' spinal cords, while 3EVs-Dxm effectively reduced the M1 pro-inflammatory phenotype and increased the M2 anti-inflammatory phenotype (Fig. 4, C and D), which was consistent with the in vitro results (Fig. 3, I to K). Also, 3EVs-Dxm-Gel showed a superior anti-inflammatory effect, with significant differences compared to both 3EVs-Dxm and SCI groups (Fig. 4E).

Further mechanism study investigated the protein levels of the spinal cord involved in the nuclear factor erythroid 2–related factor 2 (Nrf2)/heme oxygenase-1 (HO-1) and nuclear factor κB (NF-κB) pathways. The Nrf2/HO-1 pathway mediates the antioxidant effect of tissue. When sensing oxidative stress, Nrf2 dissociates from Keap1 and enters the nucleus to promote the expression of a series of antioxidant enzymes such as HO-1 (*29*). Accordingly, slightly increased expressions of Nrf2 and HO-1 were found in the spinal cords of SCI rats. In addition, 3EVs-Dxm-Gel treatment significantly up-regulated the Nrf-2/HO-1 pathway, aiding the spinal cord to alleviate oxidation damage (Fig. 4, F and G, and fig. S11).

The NF-κB pathway is a classic inflammatory pathway that mediates neuroinflammation after SCI and is involved in the M1/M2 polarization of microglial cells (*30*, *31*). After SCI, inhibitor of nuclear factor κB-α (IκB-α) is phosphorylated into p-IκB-α, is dissociated from the p65/IκB-α complex, and then undergoes ubiquitination degradation. p65 translocates into the nucleus and initiates the expression of inflammatory genes such as TNF-α and IL-1 (*32*). 3EVs-Dxm-Gel was observed to suppress the NF-κB pathway, as indicated by a decrease in the ratio of p-p65/p65 and p-IκB-α/IκB-α, thereby exerting anti-inflammatory effects (Fig. 4, F and G, and fig. S11). In summary, the constructed 3EVs-Dxm-Gel posed localized EV release for at least 1 week and sustainedly inhibited oxidation damage and inflammation in the acute phase.

3EVs-Dxm-Gel promoted functional recovery in SCI rats

The long-term efficacy was subsequently tested in the 6-week treatment in SCI rats. The body weights of rats in each group slightly decreased after surgery and then stabilized in the following weeks (Fig. 5A). Comparing the Basso, Beattie, and Bresnahan (BBB) scores of each group, 3EVs-Dxm and 3EVs-Dxm-Gel showed remarkable improvement over the SCI group in the first week. From the second week onward, the BBB scores of rats in the 3EVs-Dxm-Gel group exceeded those of the 3EVs-Dxm group (Fig. 5B). On week 6, the average BBB scores of rats were 3.33 in the SCI group, 4.5 in the 3EVs-Dxm group, 7.67 in the 3EVs-Dxm-Gel group, and 21 in the Normal group (Fig. 5C).

The toe, ankle, knee, hip, and crest of rats were labeled using marker balls, and the movement trajectories of the hindlimbs were monitored using the VICON capture camera system to assess the changes in joint angles and heights (Fig. 5D). The continuous four-gait movement trajectories presented that only the rats in the Normal and 3EVs-Dxm-Gel groups displayed a swing gait, which was indicated by red lines (Fig. 5E and movie S1). Further analysis revealed that the rats in the Normal group had a steady and large stride. SCI had a devastating impact on motor function, leading to reduced stride length even after 6-week treatments (Fig. 5F). 3EVs-Dxm effectively increased the fluctuation ranges in knee height, ankle height, and ankle angle. By contrast, rats in the 3EVs-Dxm-Gel group obtained notable improvements in both ankle and knee joint movements, as well as elevation in body-support height (Fig. 5, G to K).

In addition to the motor function recovery, the restoration of sensory function is also of great importance. The pain sense recovery of rats with different treatments was tested using mechanical and thermal stimulation. Compared with normal rats, SCI substantially reduced the pain threshold, making the rats highly sensitive to the low-scaled Von Frey fiber and thermal plate stimulations. This is consistent with the hyperalgesia caused by chronic inflammation in some SCI patients (*33*, *34*). Following the treatments with 3EVs-Dxm and 3EVs-Dxm-Gel, the sensitivities of rats to mechanical or thermal stimulation were alleviated to varying degrees. Rats treated with 3EVs-Dxm-Gel obtained better pain sense recovery (Fig. 5, L and M). We speculated that the anti-inflammatory effect of 3EVs-Dxm-Gel inhibited chronic inflammation, thereby increasing the pain threshold of rats.

3EVs-Dxm-Gel promoted tissue repair in SCI rats

Last, the neurofilament (NF) staining results showed that the rats treated with 3EVs-Dxm-Gel had the best nerve distribution in the lesion (Fig. 6, A and B), with higher nerve density and longer nerve fiber length than the SCI and 3EVs-Dxm groups (Fig. 6C). CD31 staining revealed varying degrees of vascular recovery in all rats. The rats treated with 3EVs-Dxm-Gel had more CD31-positive tubular structures in the spinal cord, indicating a higher degree of angiogenesis (Fig. 6, D and E). These tissue recoveries helped to explain the aforementioned motor and sensory improvements observed in rats of each group.

Hematoxylin and eosin–stained sections revealed that the heart, liver, spleen, lung, and kidney from all groups showed healthy morphology. No inflammatory cell infiltration or obvious pathological changes were observed, suggesting that 3EVs-Dxm-Gel has no obvious toxic side effects (fig. S12).

DISCUSSION

MSC-derived EVs are natural nanovesicles that load several types of therapeutic nucleic acids, proteins and lipids and inherit the tissue repair functions of MSCs. It has been reported that miRNA-486, miRNA-125, and miRNA-126 in EVs' cargos could reduce neuron apoptosis, promote axon regeneration, regulate microglia polarization, and enhance angiogenesis (*35*–*38*). Because of their relative ease of storage and transportation compared to MSCs, EVs have been increasingly used as substitutes for MSCs to treat SCI (*39*). Meanwhile, it has been demonstrated that 3D culture of MSCs can simulate the in vivo cell state, altering EV cargos and endowing EVs

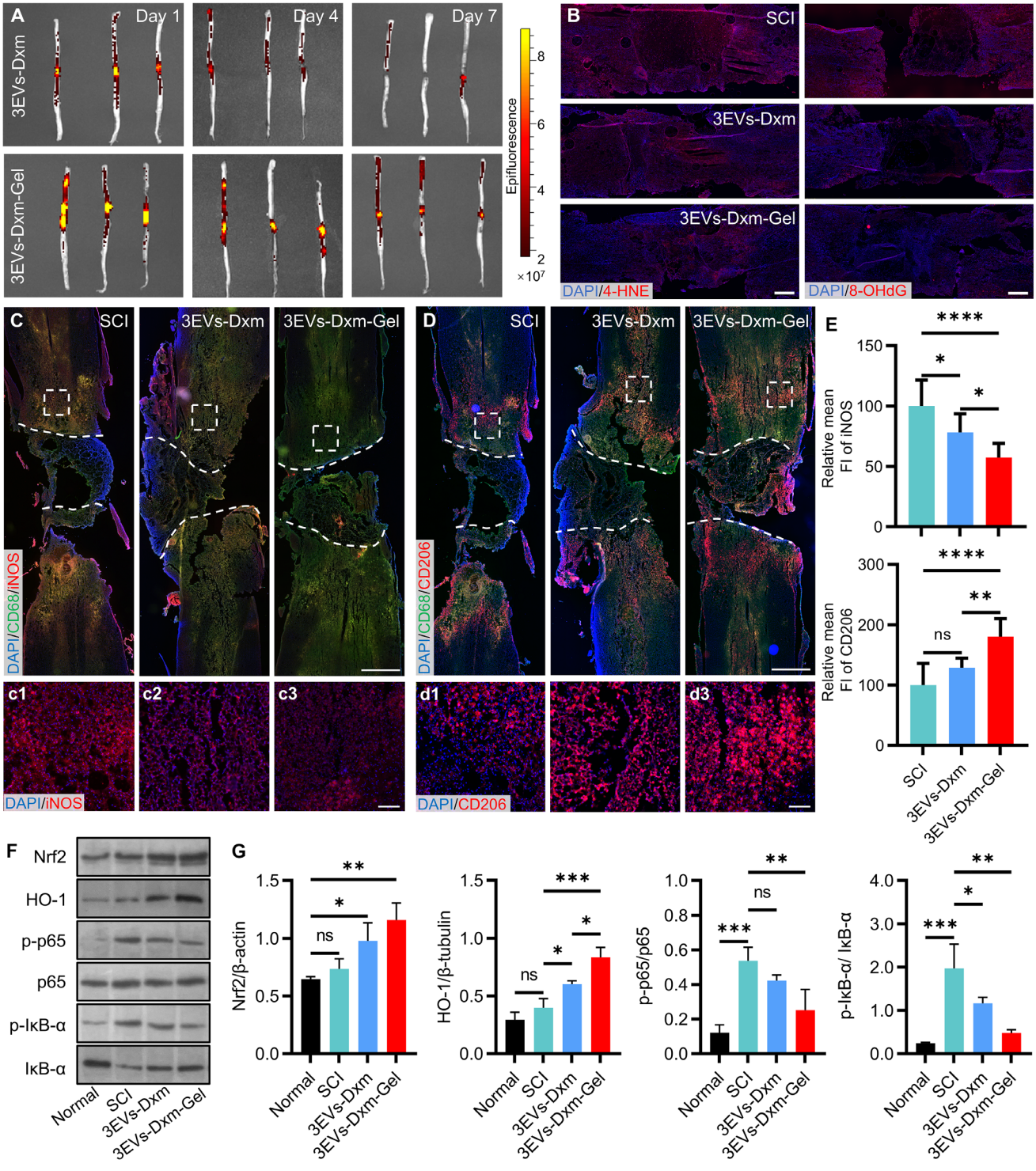

Fig. 4. In vivo fate of 3EVs-Dxm-Gel and its antioxidative and anti-inflammatory effects in SCI rats. (**A**) EV distribution after injecting 3EVs-Dxm and 3EVs-Dxm-Gel in the spinal cord for 1, 4, and 7 days. (**B**) 4-HNE and 8-OHdG levels in the spinal cord from SCI, 3EVs-Dxm, and 3EVs-Dxm-Gel groups (scale bar, 500 μm). (**C**) iNOS and (**D**) CD206 expressions of spinal cord tissues in SCI, 3EVs-Dxm, and 3EVs-Dxm-Gel groups (scale bar, 1 mm) and (**E**) their relative mean fluorescence intensity analysis ($n = 3$; three regions per section were selected for statistical analysis). [(C), 1 to (C), 3 and (D), 1 to (D), 3] are the zoomed-in images from white squares in the upper images. Scale bars, 100 μm. The white dashed lines indicate incision of spinal cord. (**F**) Nrf2, HO-1, p-p65, p65, p-IκB-α, and IκB-α expressions of the spinal cord from Normal, SCI, 3EVs-Dxm, and 3EVs-Dxm-Gel groups and (**G**) their semiquantitative analysis ($n = 3$). $^{ns}P > 0.05$, $^{*}P < 0.05$, $^{**}P < 0.01$, ***P < 0.001, and $^{****}P < 0.0001$.

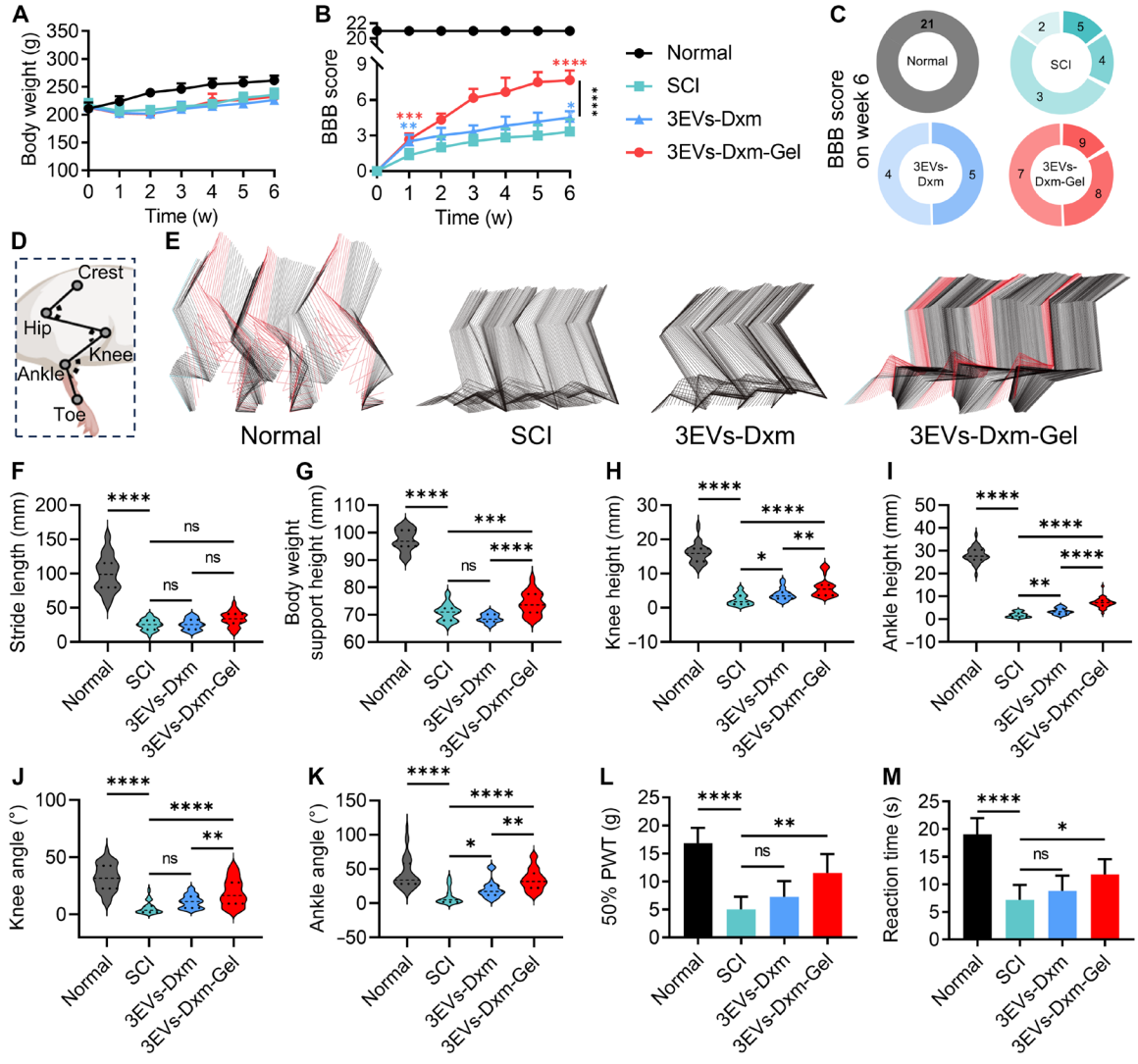

Fig. 5. Locomotor and sensory promotion effects of 3EVs-Dxm-Gel in SCI rats. (**A**) Body weight and (**B**) BBB score changes of rats in Normal, SCI, 3EVs-Dxm, and 3EVs-Dxm-Gel groups ($n = 6$). The blue or red asterisk (*) represents the statistical difference between the SCI group and the 3EVs-Dxm or 3EVs-Dxm-Gel group. w, weeks. (**C**) Pie graphs showing the distribution of BBB scores of rats on week 6. (**D**) Schematic diagram of labeled joints of hindlimb and (**E**) their trajectories during the movement within each group. The red lines refer to the swing phase, and the black lines signify the stance phase. (**F**) Stride length, (**G**) fluctuation range of body weight support height, (**H**) knee height, (**I**) ankle height, and fluctuation range of (**J**) knee angle and (**K**) ankle angle of rat hindlimbs with different treatments ($n = 3$; 12 strides of each rat were selected for statistical analysis). (**L**) 50% PWT of rats under the mechanical stimulation in Normal, SCI, 3EVs-Dxm, and 3EVs-Dxm-Gel groups ($n = 6$). (**M**) Reaction time of rats under the heat stimulation in each group ($n = 6$). $^{ns}P > 0.05$, $^{*}P < 0.05$, $^{**}P < 0.01$, $^{***}P < 0.001$, and $^{****}P < 0.0001$.

with stronger microenvironment regulatory capabilities (*22*, *40*). Yan *et al.* added different concentrations of ascorbic acid to the MSC culture medium and successfully prepared millimeter-sized MS, showing excellent EV secretion characteristics (*41*). Following Yan *et al.*'s method, we added ascorbic acid (120 μg/ml) to the culture medium and successfully fabricated MS. Compared with MSC, MS can maintain a stable spheroid shape over 1 month and thus avoid repetitive cell digestion and subculture steps, which simplified the massive extraction of EVs. The data showed that 3EVs had similar physicochemical properties including biomarkers, size, zeta potential, and morphology to 2EVs. 3EVs exhibited promoted pro-angiogenic and neurotrophic capacities, which are urgently needed in vessel and neuron recovery after SCI.

EVs play vital role in maintaining microenvironment homeostasis (*42*). In this study, we found that 3EVs inherently have anti-inflammatory activity in LPS-stimulated BV2 cells, but this is insufficient. Fortunately, the lipid bilayer structure of EVs enables them to encapsulate drugs within their hydrophilic core and hydrophobic lipid layer (*43*). Moreover, the rapid uptake of EVs by target cells facilitates the targeting delivery of drugs loaded in EVs (*44*). Therefore, loading classic anti-inflammatory drug, such as Dxm, into 3EVs would greatly enhance their anti-inflammatory effect. In this study, we used the probe sonication method, known for its simplicity, efficiency, and repeatability, to fabricate the 3EVs-Dxm. The key to this method is controlling the ultrasound energy to ensure adequate Dxm loading while avoiding damage to the EVs' structure (*45*). After screening, we

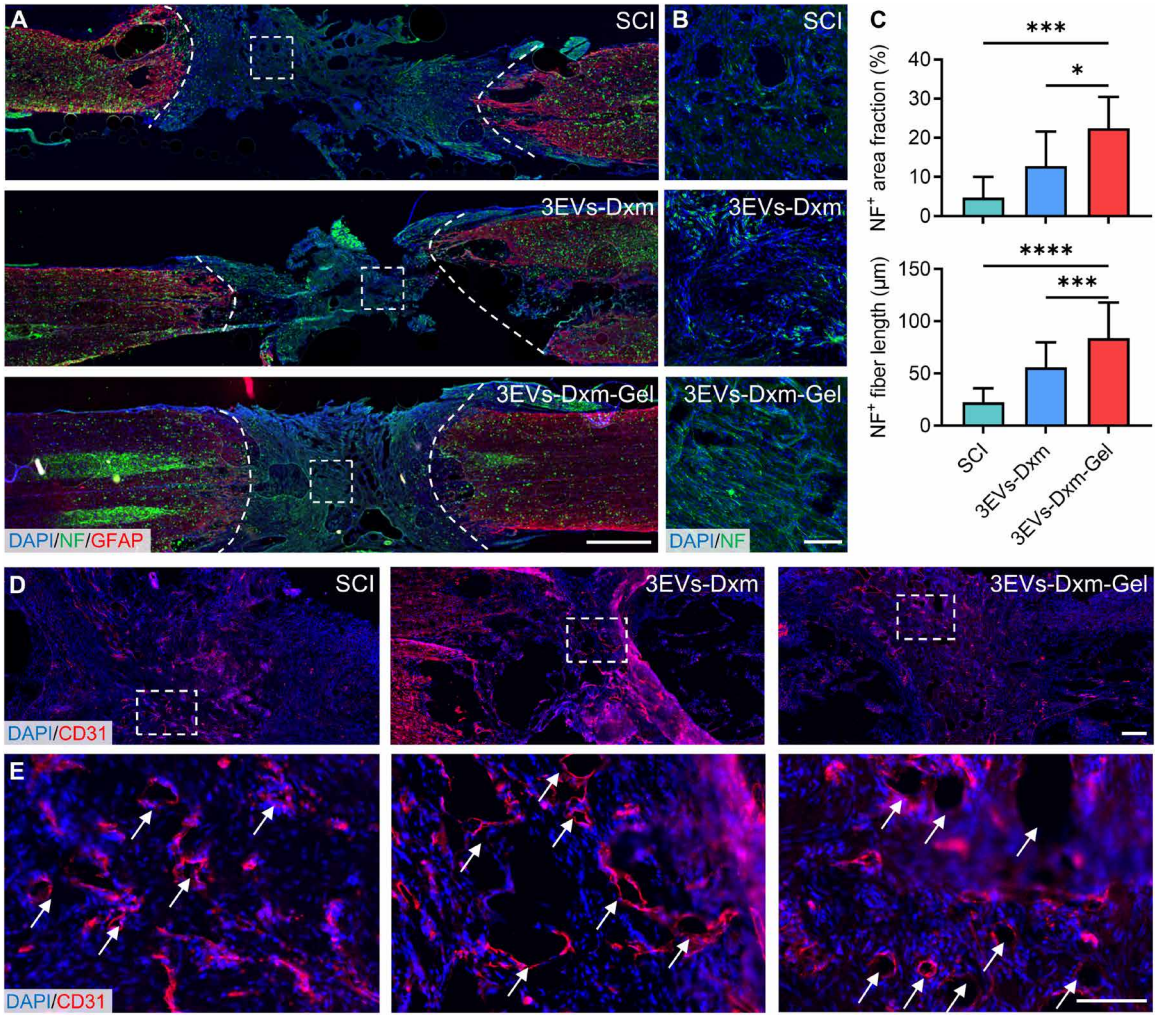

Fig. 6. Tissue recovery promoted by 3EVs-Dxm-Gel in SCI rats. (**A**) Glial fibrillary acidic protein (GFAP) and NF expressions in the spinal cord in SCI, 3EVs-Dxm, and 3EVs-Dxm-Gel groups (scale bar, 1 mm). The white dashed lines indicate the boundary of lesion. (**B**) Zoomed-in images of white squares in (A) (scale bar, 100 μm). (**C**) Quantitative analysis of NF^+ area fraction ($n = 3$; three regions per section were selected for statistical analysis) and NF^+ fiber length ($n = 3$; nine fibers per section were selected for statistical analysis) in the lesion. (**D**) CD31 expression in the spinal cord in SCI, 3EVs-Dxm, and 3EVs-Dxm-Gel groups (scale bar, 200 μm). (**E**) Zoomed-in images of white squares in (D) (scale bar, 100 μm). The white arrows present the neovascularization. *$P < 0.05$, ***$P < 0.001$, and ****$P < 0.0001$.

selected 10% sonication energy for the preparation of 3EVs-Dxm, as it achieved the highest Dxm loading content (84.61 μg per 50 μg of 3EVs) and encapsulation efficiency (26.8%) while maintaining the structure. 3EVs-Dxm can be quickly taken up by PC12 cells, HUVECs, and BV2 cells within 60 min, which accelerated the glucocorticoid receptor binding of Dxm in the cytoplasm and exerts its anti-inflammatory activities. As expected, immunofluorescence results and ELISA data suggested that 3EVs-Dxm suppressed M1 polarization and promoted M2 polarization of BV2 cells.

Over the past decades, various hydrogel delivery systems have been developed to locally and efficiently deliver EVs into the damaged spinal cord. In this way, hydrogel acts as an EV reservoir, releasing EVs in an appropriate manner to achieve continuous SCI repair. As secondary injury caused by SCI lasts for several weeks and even longer, many studies focused on how to achieve sustained EV release from hydrogel. For example, Zhu *et al.* prepared a composite hydrogel composed of nanofibers and HA to load EVs, which can be slowly released from hydrogel for 15 days in vitro (*46*). Li *et al.* used cell-adhesive peptides to attach EVs to an HA hydrogel, enabling a slow release of EVs over 11 days (*47*). Although sustained release endows EVs continuous regulation of the SCI microenvironment, the neuroinflammation and oxidative damage following SCI are dynamically changing (*14*), which requires on-demand treatment. Constructing a hydrogel system to release loaded EVs in response to pathological progression may address this issue. Previous studies suggested that ROS can reflect the severity of SCI and can be used as a trigger for a responsive hydrogel (*48*). This study modified 3EVs-Dxm with -2OH and grafted them with HA-PBA to form a covalent linkage, PBA ester. By this way, 3EVs-Dxm can be immobilized within the hydrogel, shielding them from the washout and diffusion by blood and cerebrospinal fluid. The ROS sensitivity of the PBA ester optimized the release pattern of EVs, realizing on-demand regulation of the microenvironment. In vitro studies confirmed the ROS-responsive release of 3EVs-Dxm from 3EVs-Dxm-Gel. The EV

release from 3EVs-Dxm-Gel lasted over 1 week in SCI rats and improved the antioxidative and anti-inflammatory efficacies compared to direct injection of 3EVs-Dxm. Such early intervention would ameliorate the inhibitory microenvironment, facilitating neuronal survival and later recovery (*49*). The pathology of SCI involves chain reactions with various cellular and molecular pathological alterations (*15*). Hence, the desirable neural repair and functional recovery following SCI often require a comprehensive treatment. In this study, 3EVs-Dxm-Gel provided a multidimension treatment, which remarkably improved motor function and pain sense recovery. In summary, this approach provided insights into the EV delivery and treatment strategy for central nervous system injury.

Despite the substantial therapeutic effects observed in rats treated with 3EVs-Dxm-Gel, a substantial gap in terms of functional and tissue recovery compared to normal rats remained. In this study, the hydrogel delivery system realized the efficient delivery of EVs to the injury site during the acute phase but still struggled to achieve long-term and flexible treatments regarding specific conditions of SCI. In future research, we will combine hydrogel implantation with systemic administration to achieve rapid treatment during the acute phase and flexible treatment during the intermediate and chronic phases.

MATERIALS AND METHODS

Materials

3-Amino-2-hydroxypropanol, ascorbic acid, LPS, and NGF were purchased from Merck Life Science (Darmstadt, Germany). 2-Amino phenylboronic acid and 1-hydroxybenzotriazole were obtained from Yuanye Bio-Technology (Shanghai, China). HA was sourced from Bloomage Biotechnology (Jinan, China). DSPE-PEG_{5000}-NHS was provided by Ponsure Biotechnology (Shanghai, China). TA, 1-(3-dimethylaminopropyl)-3-ethylcarbodiimide, and Hepes buffer were obtained from Macklin Inc. (Shanghai, China). Dxm, H_2O_2, DPPH free radical scavenging capacity assay kit, and DiI were purchased from Solarbio Science & Technology (Beijing, China). MicroBCA kit was bought from Thermo Fisher Scientific (Shanghai, China). TNF-α, IL-6, IL-4, and IL-10 ELISA kits were purchased from Multisciences Biotech (Hangzhou, China). Calcein AM, propidium iodide, and 2′,7′-dichlorodihydrofluorescein diacetate were acquired from Beyotime Inc. (Shanghai, China).

Cells and animals

BV2 cells, PC12 cells, and HUVECs were obtained from iCell Bioscience Inc. (Shanghai, China). Human umbilical cord MSCs (ethics code: 2021-R108) were provided by SinoCell Technology Co., Ltd. (Ningbo, China).

Female Sprague-Dawley rats weighing between 220 and 250 g were acquired from SLAC Laboratory Animal Co., Ltd. (Shanghai, China). All experiments involving animals were conducted following the guidelines set by the Animal Ethics Committee of Zhejiang University (ethics approval code: ZJU20210136).

MS preparation and 3EVs extraction

MSCs were cultured in BC-T4 medium (Zhuhai Baso Cell Science&Technology Co., Ltd., China) supplemented with 10% serum substitute (AventaCell, US). MSCs (1×10^6 cells per well) were seeded into a six-well plate and allowed to adhere overnight. The medium was then replaced with fresh culture medium containing ascorbic acid (120 μg/ml). After 2 days of culture, the MSCs formed a thin film at the bottom of the plate. The edges of the film were detached using sterile tweezers and cultured for another 3 days, during which MS spontaneously formed. The morphology of MS was observed using SEM. The MS was transferred to a culture flask. The medium was collected every 3 days for EV extraction, and fresh medium was added.

The collected medium was centrifuged at 3000*g* for 6 min to remove cell debris and impurities and then concentrated to 100 ml using a tangential flow filtration system (Sartorius, Germany) with a 100-kDa molecular weight cutoff (MWCO). The concentrated medium was centrifuged (10,000*g*) for 1 hour, and the supernatant was subjected to ultracentrifugation (100,000*g*) using an ultracentrifuge (Allegra-64R, Beckman Coulter Life Science, US) for 1 hour. The pellet was washed using sterile PBS solution and centrifuged at 100,000*g* for 1 hour again.

The pellet was then resuspended in 1 ml of sterile PBS for storage. The quantity of 3EVs was determined by measuring the protein content using a microBCA kit. As a control, the culture medium of 2D MSCs was collected for 2EVs extraction.

Characterization of 2EVs and 3EVs

2EVs (200 μg/ml) and 3EVs (200 μg/ml) were placed on copper grids and negatively stained using uranyl acetate. EVs' morphology was scanned using TEM (Talos L120C, Thermo Fisher Scientific, US). The particle sizes and zeta potentials were determined using a nanoparticle analyzer (Nano-ZS90, Malvern, UK). The biomarkers of 2EVs and 3EVs, including CD9 (SC-13118, Santa Cruz Biotechnology), CD63 (SC-365604, Santa Cruz Biotechnology), and TSG101 (SC-7964, Santa Cruz Biotechnology), were detected using WB.

Pro-angiogenic and neurotrophic capacities of 3EVs

The two-well silicon inserts (ibidi, Germany) were sterilized using 75% ethanol and then fixed in a 24-well plate. Seventy microliters of prepared HUVEC suspension (5×10^5 cells/ml) was added to the inserts. After overnight incubation, the inserts were carefully removed to create uniform-width cell scratches. The medium was then refreshed with a culture medium containing 2EVs or 3EVs (30 μg/ml). HUVEC migration was observed every 5 hours, and images were captured using an optical microscope (ECLIPSE Ti system, Nikon, Japan).

Standard Matrigel (354230, Corning, US) was added vertically in 24-well plates (200 μl per well). The plates were gently shaken and incubated at 37°C for 1 hour for gelation. HUVEC suspensions (1.2×10^5 cells/ml) were prepared using a medium containing either 2EVs or 3EVs (30 μg/ml) and were added to the Matrigel-coated plates (500 μl per well). Tube formation was observed every 2 hours, and images were captured.

PC12 cells were seeded at a density of 1×10^4 cells per well in a confocal cell dish (SAINING Biotechnology, China) for 24 hours. The medium was replaced with a fresh medium containing 1% fetal bovine serum and NGF (100 ng/ml). Next, 2EVs or 3EVs (50 μg/ml) were added to the culture medium. The differentiation status of the cells was monitored daily. On day 3, the cells were labeled with calcein AM, and cell images were captured using a confocal microscope (TCS SP8, Leica, Germany).

Preparation and optimization of 3EVs-Dxm

Dxm and 3EVs were added to PBS to achieve concentrations of 200 and 50 μg/ml, respectively. The mixture was placed on ice and subjected to probe sonication (KQ5200B, Kunshan Ultrasonic

Instrument Co., Ltd., China) with the following settings: 0 to 15% energy (maximum power, 650 W), five cycles, 3 min per cycle with 15 s on/off, and 2 min of interval between cycles. The EV suspension was then incubated in a 37°C water bath for 1 hour to facilitate the recovery of the EVs' membrane postsonication. The EV suspension was then ultracentrifuged at 100,000*g* for 1 hour, washed with PBS, and ultracentrifuged again at 100,000*g* for 1 hour to obtain 3EVs-Dxm. HPLC (LC-20ADXR, SHIMADZU, Japan) was used to determine the drug content and encapsulation efficiency of 3EVs-Dxm. The HPLC settings were as follows: Mobile phases were 70% methanol and 30% water, the flow rate was 1 ml/min, the scan time was 10 min, the column temperature was 25°C, and the absorbance wavelength was 240 nm. To optimize drug encapsulation, different ultrasound energies (0, 5, 10, and 15%) were used for 3EVs-Dxm construction and were evaluated via drug contents, encapsulation efficiency, particle sizes, zeta potentials, and TEM images.

Anti-inflammatory effect of 3EVs-Dxm

To detect the cell uptake of 3EVs-Dxm, BV2 cells, PC12 cells, and HUVECs (10^5 cells per well) were seeded in 24-well plates and incubated for 24 hours. BV2 cells were prestimulated with LPS (100 ng/ml) for 4 hours before measurement. DiI-labeled 3EVs-Dxm (20 μg/ml) was added into the culture medium of all three cell types, and the cells were digested and collected into flow cytometry tubes at 0, 30, and 60 min. The cells were fixed, and cell uptake was measured using flow cytometry (CytoFLEX LX, Beckman Coulter Life Science, US) to determine the cell uptake at each time point.

BV2 cells were seeded in a 24-well plate (8×10^4 cells per well). After overnight adherence, the medium was refreshed with fresh medium (blank group), medium containing LPS (100 ng/ml), medium containing LPS (100 ng/ml) and Dxm (85 μg/ml), medium containing LPS (100 ng/ml) and 3EVs (50 μg/ml), and medium containing LPS (100 ng/ml) and 3EVs-Dxm (50 μg/ml). After 48 hours of incubation, the medium was collected for cytokine measurement including TNF-α, IL-6, IL-4, and IL-10 using ELISA kits. The cells were fixed with 4% paraformaldehyde and washed with PBS for immunofluorescence assay. Then, the cells were successively permeabilized using Triton X-100 (0.2%), blocked using goat serum, and stained using primary antibodies including iNOS (ab178945, Abcam, US) and CD206 (24595, Cell Signaling Technology, US). After overnight incubation, excess primary antibodies were washed with PBS, and the cells were stained with fluorescence-conjugated secondary antibodies (Yeasen Biotechnology, China). Last, DAPI (4′,6-diamidino-2-phenylindole) was added to label the nuclei, and the cells were observed using a confocal microscope. For semiquantitative analysis, multiple regions from cell images in each group were randomly selected, and the mean fluorescence intensity of iNOS or CD206 was measured using ImageJ software.

Synthesis of HA-PBA and DSPE-PEG_{5000}-2OH

2-Aminophenylboronic acid (43 mg) was added in 20 ml of HA solution (5 mg/ml). Subsequently, 48 mg of 1-(3-dimethylaminopropyl)-3-ethylcarbodiimide and 34 mg of 1-hydroxybenzotriazole dissolved in dimethyl sulfoxide were added into the HA solution (pH 5). The mixture was reacted at room temperature for 48 hours and dialyzed (MWCO: 8 kDa) against ultrapure water for 3 days. Last, the purified product was frozen at −80°C and lyophilized to obtain HA-PBA.

One hundred milligrams of DSPE-PEG_{5000}-NHS and 5 mg of -2OH were dissolved in Hepes buffer (pH 8 to 9) and allowed to react at room temperature for 8 hours. The reaction solution was dialyzed (MWCO: 3 kDa) against ultrapure water for 2 days. The purified product was lyophilized to obtain DSPE-PEG_{5000}-2OH.

To confirm the chemical structure, HA-PBA was dissolved in deuterium oxide (D_2O). DSPE-PEG_{5000}-NHS, -2OH, and DSPE-PEG_{5000}-2OH were dissolved in deuterated methanol. All samples were scanned using a nuclear magnetic resonance spectrometer (Bruker Technology, Beijing, China).

Construction of 3EVs-Dxm-Gel

DSPE-PEG_{5000}-2OH (2 mg/ml) and 3EVs-Dxm (100 μg/ml) were added in 1 ml of PBS and incubated at 37°C for 60 min. The suspension was ultracentrifuged twice (100,000*g*, 60 min) to remove the free DSPE-PEG_{5000}-2OH.

To assess the modification ratio of 3EVs-Dxm, fluorescently labeled DSPE-PEG_{5000}-Cy5 was co-incubated with 3EVs-Dxm using the same procedure. At 0, 30, and 60 min of co-incubation, the free dye was removed by ultracentrifugation (100,000*g*, 60 min) twice. The modified 3EVs-Dxm were then dispersed in 1 ml of PBS and detected using a Flow NanoAnalyzer (N30, Xiamen Fuliu Biotechnology, China).

To construct 3EVs-Dxm-Gel, the modified 3EVs-Dxm were resuspended in HA-PBA solution (40 mg/ml) and incubated at room temperature for 30 min. An equal volume of TA solution (10 mg/ml) was then added to form an EV-integrated hydrogel (3EVs-Dxm-Gel). The mechanical property of 3EVs-Dxm-Gel was assessed with a rheometer (MaRG 40, Thermo Fisher Scientific, US).

EV release of 3EVs-Dxm-Gel and its antioxidative effect

3EVs-Dxm-Gel was placed in 5 ml of PBS solution or H_2O_2 (1 mM) solution. At 0, 1, 2, 4, 8, 16, 24, 36, 48, 72, 96, 120, and 144 hours, 200 μl of solution was collected, and 200 μl of fresh PBS or H_2O_2 solution was added. The release amount of EVs was measured using a microBCA assay kit. Fresh H_2O_2 was added daily to maintain its concentration. As a control, the unmodified 3EVs-Dxm were mixed with HA-PBA, incubated for 30 min, and then cross-linked with TA to form a gel. Likewise, 3EVs-Dxm + Gel was placed in PBS or H_2O_2 (1 mM) solutions to detect EV release. Hydrogel degradation was observed daily.

To investigate the antioxidative effect, 3EVs-Dxm-Gel and its components were separately added into 1 ml of DPPH solution (40 μg/ml) to observe the color change. The solutions were then transferred to a 96-well plate (200 μl per well), and the optical density value was measured at 490 nm.

Oxidation damage was induced in PC12 cells using H_2O_2. PC12 cells in six-well plates (6×10^5 cells per well) were co-incubated with 200 μM H_2O_2 and 3EVs-Dxm or 3EVs-Dxm-Gel for 24 hours. All cells were collected to incubate with 2′,7′-dichlorodihydrofluorescein diacetate at 37°C for 20 min. The cells were subsequently washed twice and resuspended in PBS for flow cytometry analysis.

Short-term therapeutic efficacy of 3EVs-Dxm-Gel in SCI rats

The Sprague-Dawley rats were anesthetized and weighed, and their back hair was shaved. After the sterilization of the skin, a laminectomy was performed at the T9-T10 vertebral level to expose the spinal cord. The spinal cord was then fully transected to form a lesion (3 mm). The back muscles and skin were successively sutured. Post-SCI, the rats were weak and required daily manual urination and penicillin injections.

For short-term efficacy evaluation, the SCI rats were injected with PBS solution (SCI group), 200 μg of 3EVs-Dxm (3EVs-Dxm group), or 3EVs-Dxm-Gel containing 200 μg of 3EVs-Dxm (3EVs-Dxm-Gel group). The injection volume was 80 μl. On day 1, 4, and 7, the rats were euthanized, and their spinal cords were collected to detect the in vivo distribution of EVs using a live imaging system (IVIS Spectrum, PerkinElmer, US).

On day 4, the spinal cord was collected and an immunofluorescence assay was conducted to detect 4-HNE (ab48506, Abcam, US), 8-OHdG (OM176273, Omini mAbs, US), iNOS, and CD206. In addition, WB was used to measure the Nrf2 (ab92946, Abcam, US), HO-1 (ab68477, Abcam, US), IκB (4812, Cell Signaling Technology, US), p-IκB (2859, Cell Signaling Technology, US), p65 (8242, Cell Signaling Technology, US), and p-p65 (3033, Cell Signaling Technology, US) expressions. For the semiquantitative analysis of iNOS and CD206, multiple regions in CD68-positive area adjacent to the spinal cord lesion were selected and their mean fluorescence intensity was measured using ImageJ software.

Long-term therapeutic efficacy of 3EVs-Dxm-Gel in SCI rats

The SCI rats were divided into the SCI, 3EVs-Dxm, and 3EVs-Dxm-Gel groups. The rats were weighed and recorded weekly. The performance of free walking in the open field was scored according to the BBB scale. On week 6, the rats' hindlimbs were shaved and depilated. The joints were labeled using marker balls, and their motions were observed using the VICON capture camera system. The data were exported using NEXUS software and analyzed using Python and MATLAB software.

For pain sense assessment, Von Frey filaments with forces of 0.4, 1.0, 2.0, 4.0, 6.0, 8.0, 10, and 15.0 g were used to apply mechanical stimulation to the plantar region of the rats' hind paws. A quick paw withdrawal or licking response was recorded as positive and marked as "X"; no response was recorded as negative and marked as "O." The testing began with a 2.0-g filament. If the response was negative, a filament with a higher force was used; if the response was positive, a filament with a lower force was used. Each rat was tested five times after the first appearance of the XO or OX pattern, with a 30-s interval between each test. The results of the five tests ("O" or "X") and the scale of the filament used in the final test were noted. The 50% paw withdrawal threshold (50% PWT) was calculated. In another experiment, rats were placed on a heated plate (55°C), ensuring that the plantar was in contact with the plate. The time taken for the rats to exhibit a paw withdrawal or licking response was recorded. If no response was observed within 30 s, the test was terminated to prevent irreversible thermal injury, and the time was recorded as 30 s.

Following the evaluation of locomotor function and pain sensation, the rats were humanely euthanized, and their spinal cords were subsequently harvested to detect the expression levels of glial fibrillary acidic protein (GFAP; BA0056, BOSTER Biological Technology, China), NF (2836, Cell Signaling Technology, US), and CD31 (ab222783, Abcam, US) in the spinal cords of each group using an immunofluorescence assay. In addition, the heart, liver, spleen, lung, and kidneys were prepared as paraffin sections and subjected to hematoxylin and eosin staining.

Statistical analysis

The data were expressed as the means ± SD and statistically evaluated using Student's *t* test for the comparisons between two groups and one-way analysis of variance (ANOVA) for multiple group analyses. A P value below 0.05 was deemed statistically significant ($^{ns}P > 0.05$, $^{*}P < 0.05$, $^{**}P < 0.01$, $^{***}P < 0.001$, and $^{****}P < 0.0001$).

Supplementary Materials

The PDF file includes:

Figs. S1 to S12

Legend for movie S1

Other Supplementary Material for this manuscript includes the following:

Movie S1

REFERENCES AND NOTES

1. C. S. Ahuja, J. R. Wilson, S. Nori, M. R. N. Kotter, C. Druschel, A. Curt, M. G. Fehlings, Traumatic spinal cord injury. *Nat. Rev. Dis. Primers.* **3**, 17018 (2017).
2. A. M. Rubiano, N. Carney, R. Chesnut, J. C. Puyana, Global neurotrauma research challenges and opportunities. *Nature* **527**, S193–S197 (2015).
3. B. Guan, D. B. Anderson, L. Chen, S. Feng, H. Zhou, Global, regional and national burden of traumatic brain injury and spinal cord injury, 1990–2019: A systematic analysis for the Global Burden of Disease Study 2019. *BMJ Open* **13**, e075049 (2023).
4. GBD Spinal Cord Injuries Collaborators, Global, regional, and national burden of spinal cord injury, 1990–2019: A systematic analysis for the Global Burden of Disease Study 2019. *Lancet Neurol.* **22**, 1026–1047 (2023).
5. B. Zheng, M. H. Tuszynski, Regulation of axonal regeneration after mammalian spinal cord injury. *Nat. Rev. Mol. Cell Biol.* **24**, 396–413 (2023).
6. P. Assinck, G. J. Duncan, B. J. Hilton, J. R. Plemel, W. Tetzlaff, Cell transplantation therapy for spinal cord injury. *Nat. Neurosci.* **20**, 637–647 (2017).
7. B. Fan, Z. Wei, S. Feng, Progression in translational research on spinal cord injury based on microenvironment imbalance. *Bone Res.* **10**, 35 (2022).
8. O. Levy, R. Kuai, E. M. J. Siren, D. Bhere, Y. Milton, N. Nissar, M. De Biasio, M. Heinelt, B. Reeve, R. Abdi, M. Alturki, M. Fallatah, A. Almalik, A. H. Alhasan, K. Shah, J. M. Karp, Shattering barriers toward clinically meaningful MSC therapies. *Sci. Adv.* **6**, eaba6884 (2020).
9. H. Huang, W. Young, S. Skaper, L. Chen, G. Moviglia, H. Saberi, Z. Al-Zoubi, H. S. Sharma, D. Muresanu, A. Sharma, W. El Masry, S. Feng, International Association of Neurorestoratology and The Chinese Association of Neurorestoratology, Clinical neurorestorative therapeutic guidelines for spinal cord injury (IANR/CANR version 2019). *J. Orthop. Translat.* **20**, 14–24 (2020).
10. M. D. Hade, C. N. Suire, Z. Suo, Mesenchymal stem cell-derived exosomes: Applications in regenerative medicine. *Cells* **10**, 1959 (2021).
11. Y. Shen, J. Cai, The importance of using exosome-loaded miRNA for the treatment of spinal cord injury. *Mol. Neurobiol.* **60**, 447–459 (2023).
12. D. Buschmann, V. Mussack, J. B. Byrd, Separation, characterization, and standardization of extracellular vesicles for drug delivery applications. *Adv. Drug Deliv. Rev.* **174**, 348–368 (2021).
13. Q. Li, X. Fu, Y. Kou, N. Han, Engineering strategies and optimized delivery of exosomes for theranostic application in nerve tissue. *Theranostics* **13**, 4266–4286 (2023).
14. E. J. Bradbury, E. R. Burnside, Moving beyond the glial scar for spinal cord repair. *Nat. Commun.* **10**, 3879 (2019).
15. C. Li, Z. Wu, L. Zhou, J. Shao, X. Hu, W. Xu, Y. Ren, X. Zhu, W. Ge, K. Zhang, J. Liu, R. Huang, J. Yu, D. Luo, X. Yang, W. Zhu, R. Zhu, C. Zheng, Y. E. Sun, L. Cheng, Temporal and spatial cellular and molecular pathological alterations with single-cell resolution in the adult spinal cord after injury. *Signal Transduct. Target. Ther.* **7**, 65 (2022).
16. L. Yang, J. Cao, Y. Du, X. Zhang, W. Hong, B. Peng, J. Wu, Q. Weng, J. Wang, J. Gao, Initial IL-10 production dominates the therapy of mesenchymal stem cell scaffold in spinal cord injury. *Theranostics* **14**, 879–891 (2024).
17. L. M. Marquardt, V. M. Doulames, A. T. Wang, K. Dubbin, R. A. Suhar, M. J. Kratochvil, Z. A. Medress, G. W. Plant, S. C. Heilshorn, Designer, injectable gels to prevent transplanted Schwann cell loss during spinal cord injury therapy. *Sci. Adv.* **6**, eaaz1039 (2020).
18. L. Fan, C. Liu, X. Chen, Y. Zou, Z. Zhou, C. Lin, G. Tan, L. Zhou, C. Ning, Q. Wang, Directing induced pluripotent stem cell derived neural stem cell fate with a three-dimensional biomimetic hydrogel for spinal cord injury repair. *ACS Appl. Mater. Interfaces* **10**, 17742–17755 (2018).
19. M. Pu, H. Cao, H. Zhang, T. Wang, Y. Li, S. Xiao, Z. Gu, ROS-responsive hydrogels: From design and additive manufacturing to biomedical applications. *Mater. Horiz.* **11**, 3721–3746 (2024).

20. Y. Cao, Y. Xu, C. Chen, H. Xie, H. Lu, J. Hu, Local delivery of USC-derived exosomes harboring ANGPTL3 enhances spinal cord functional recovery after injury by promoting angiogenesis. *Stem Cell Res. Ther.* **12**, 20 (2021).
21. X. Hu, W. Xu, Y. Ren, Z. Wang, X. He, R. Huang, B. Ma, J. Zhao, R. Zhu, L. Cheng, Spinal cord injury: Molecular mechanisms and therapeutic interventions. *Signal Transduct. Target. Ther.* **8**, 245 (2023).
22. M. Han, H. Yang, X. Lu, Y. Li, Z. Liu, F. Li, Z. Shang, X. Wang, X. Li, J. Li, H. Liu, T. Xin, Three-dimensional-cultured MSC-derived exosome-hydrogel hybrid microneedle array patch for spinal cord repair. *Nano Lett.* **22**, 6391–6401 (2022).
23. V. S. Madamsetty, R. Mohammadinejad, I. Uzieliene, N. Nabavi, A. Dehshahri, J. García-Couce, S. Tavakol, S. Moghassemi, A. Dadashzadeh, P. Makvandi, A. Pardakhty, A. Aghaei Afshar, A. Seyfoddin, Dexamethasone: Insights into pharmacological aspects, therapeutic mechanisms, and delivery systems. *ACS Biomater Sci. Eng.* **8**, 1763–1790 (2022).
24. Y. Li, X. He, R. Kawaguchi, Y. Zhang, Q. Wang, A. Monavarfeshani, Z. Yang, B. Chen, Z. Shi, H. Meng, S. Zhou, J. Zhu, A. Jacobi, V. Swarup, P. G. Popovich, D. H. Geschwind, Z. He, Microglia-organized scar-free spinal cord repair in neonatal mice. *Nature* **587**, 613–618 (2020).
25. P. Guan, C. Liu, D. Xie, S. Mao, Y. Ji, Y. Lin, Z. Chen, Q. Wang, L. Fan, Y. Sun, Exosome-loaded extracellular matrix-mimic hydrogel with anti-inflammatory property facilitates/promotes growth plate injury repair. *Bioact. Mater.* **10**, 145–158 (2022).
26. L. Xin, X. Lin, F. Zhou, C. Li, X. Wang, H. Yu, Y. Pan, H. Fei, L. Ma, S. Zhang, A scaffold laden with mesenchymal stem cell-derived exosomes for promoting endometrium regeneration and fertility restoration through macrophage immunomodulation. *Acta Biomater.* **113**, 252–266 (2020).
27. H. Jafari, P. Ghaffari-Bohlouli, S. V. Niknezhad, A. Abedi, Z. Izadifar, R. Mohammadinejad, R. S. Varma, A. Shavandi, Tannic acid: A versatile polyphenol for design of biomedical hydrogels. *J. Mater. Chem. B* **10**, 5873–5912 (2022).
28. Q. Ma, X. Zhao, A. Shi, J. Wu, Bioresponsive functional phenylboronic acid-based delivery system as an emerging platform for diabetic therapy. *Int. J. Nanomedicine* **16**, 297–314 (2021).
29. H. C. Huang, T. Nguyen, C. B. Pickett, Regulation of the antioxidant response element by protein kinase C-mediated phosphorylation of NF-E2-related factor 2. *Proc. Natl. Acad. Sci. U.S.A.* **97**, 12475–12480 (2000).
30. W. Liu, Y. Rong, J. Wang, Z. Zhou, X. Ge, C. Ji, D. Jiang, F. Gong, L. Li, J. Chen, S. Zhao, F. Kong, C. Gu, J. Fan, W. Cai, Exosome-shuttled miR-216a-5p from hypoxic preconditioned mesenchymal stem cells repair traumatic spinal cord injury by shifting microglial M1/M2 polarization. *J. Neuroinflammation* **17**, 47 (2020).
31. H. Fan, H. B. Tang, L. Q. Shan, S. C. Liu, D. G. Huang, X. Chen, Z. Chen, M. Yang, X. H. Yin, H. Yang, D. J. Hao, Quercetin prevents necroptosis of oligodendrocytes by inhibiting macrophages/microglia polarization to M1 phenotype after spinal cord injury in rats. *J. Neuroinflammation* **16**, 206 (2019).
32. H. Yu, L. Lin, Z. Zhang, H. Zhang, H. Hu, Targeting NF-κB pathway for the therapy of diseases: Mechanism and clinical study. *Signal Transduct. Target. Ther.* **5**, 209 (2020).
33. N. B. Finnerup, I. L. Johannesen, A. Fuglsang-Frederiksen, F. W. Bach, T. S. Jensen, Sensory function in spinal cord injury patients with and without central pain. *Brain* **126**, 57–70 (2003).
34. L. Wang, M. A. Gunduz, A. T. Semeano, E. C. Yılmaz, F. A. H. Alanazi, O. B. Imir, U. Yener, C. A. Arbelaez, E. Usuga, Y. D. Teng, Coexistence of chronic hyperalgesia and multilevel neuroinflammatory responses after experimental SCI: A systematic approach to profiling neuropathic pain. *J. Neuroinflammation* **19**, 264 (2022).
35. M. K. Jee, J. S. Jung, J. I. Choi, J. A. Jang, K. S. Kang, Y. B. Im, S. K. Kang, MicroRNA 486 is a potentially novel target for the treatment of spinal cord injury. *Brain* **135**, 1237–1252 (2012).
36. Q. Chang, Y. Hao, Y. Wang, Y. Zhou, H. Zhuo, G. Zhao, Bone marrow mesenchymal stem cell-derived exosomal microRNA-125a promotes M2 macrophage polarization in spinal cord injury by downregulating IRF5. *Brain Res. Bull.* **170**, 199–210 (2021).
37. J. Hu, L. Zeng, J. Huang, G. Wang, H. Lu, miR-126 promotes angiogenesis and attenuates inflammation after contusion spinal cord injury in rats. *Brain Res.* **1608**, 191–202 (2015).
38. Y. Zhang, Y. Xie, Z. Hao, P. Zhou, P. Wang, S. Fang, L. Li, S. Xu, Y. Xia, Umbilical mesenchymal stem cell-derived exosome-encapsulated hydrogels accelerate bone repair by enhancing angiogenesis. *ACS Appl. Mater. Interfaces* **13**, 18472–18487 (2021).
39. W. Z. Liu, Z. J. Ma, J. R. Li, X. W. Kang, Mesenchymal stem cell-derived exosomes: Therapeutic opportunities and challenges for spinal cord injury. *Stem Cell Res. Ther.* **12**, 102 (2021).
40. R. A. Haraszti, R. Miller, M. Stoppato, Y. Y. Sere, A. Coles, M. C. Didiot, R. Wollacott, E. Sapp, M. L. Dubuke, X. Li, S. A. Shaffer, M. DiFiglia, Y. Wang, N. Aronin, A. Khvorova, Exosomes produced from 3D cultures of MSCs by tangential flow filtration show higher yield and improved activity. *Mol. Ther.* **26**, 2838–2847 (2018).
41. J. Yan, L. Zhang, L. Li, W. He, W. Liu, Developmentally engineered bio-assemblies releasing neurotrophic exosomes guide in situ neuroplasticity following spinal cord injury. *Mater. Today Bio.* **16**, 100406 (2022).
42. K. Zhang, K. Cheng, Stem cell-derived exosome versus stem cell therapy. *Nat. Rev. Bioeng.* **1**, 608–609 (2023).
43. J. Wang, D. Chen, E. A. Ho, Challenges in the development and establishment of exosome-based drug delivery systems. *J. Control. Release* **329**, 894–906 (2021).
44. F. H. Brennan, Y. Li, C. Wang, A. Ma, Q. Guo, Y. Li, N. Pukos, W. A. Campbell, K. G. Witcher, Z. Guan, K. A. Kigerl, J. C. E. Hall, J. P. Godbout, A. J. Fischer, D. M. McTigue, Z. He, Q. Ma, P. G. Popovich, Microglia coordinate cellular interactions during spinal cord repair in mice. *Nat. Commun.* **13**, 4096 (2022).
45. Z. Chen, M. Xiong, J. Q. Tian, D. D. Song, S. Y. Duan, L. Zhang, Encapsulation and assessment of therapeutic cargo in engineered exosomes: A systematic review. *J. Nanobiotechnol.* **22**, 18 (2024).
46. B. Zhu, G. Gu, J. Ren, X. Song, J. Li, C. Wang, W. Zhang, Y. Huo, H. Wang, L. Jin, S. Feng, Z. Wei, Schwann cell-derived exosomes and methylprednisolone composite patch for spinal cord injury repair. *ACS Nano* **17**, 22928–22943 (2023).
47. L. Li, Y. Zhang, J. Mu, J. Chen, C. Zhang, H. Cao, J. Gao, Transplantation of human mesenchymal stem-cell-derived exosomes immobilized in an adhesive hydrogel for effective treatment of spinal cord injury. *Nano Lett.* **20**, 4298–4305 (2020).
48. D. Ma, H. Shen, F. Chen, W. Liu, Y. Zhao, Z. Xiao, X. Wu, B. Chen, J. Lu, D. Shao, J. Dai, Inflammatory microenvironment-responsive nanomaterials promote spinal cord injury repair by targeting IRF5. *Adv. Healthc. Mater.* **11**, e2201319 (2022).
49. Y. Li, Q. Zhang, Z. Liu, C. Fu, J. Ding, Microenvironments-modulated biomaterials enhance spinal cord injury therapy. *Adv. Funct. Mater.* **34**, 2403900 (2024).

Acknowledgments: We are thankful for the technical support from J. Pan and D. Wu of the Research and Service Center (College of Pharmaceutical Science, Zhejiang University) and the technical assistance provided by the core facility platform at the Zhejiang University School of Medicine. **Funding:** This work was supported by National Key Research and Development Project for Stem Cell and Transformational Research [2019YFA0112100 and 2019YFA0112102 (to J.-Q.G.)] and National Natural Science Foundation of China [81973252 (to J.-Q.G.) and 52233013 (to Z.G.)]. **Author contributions:** Conceptualization: J.C., X.Z., Z.G., and J.-Q.G. Methodology: J.C., X.Z., J.G., and J.W. Investigation: J.C., J.M., T.H., M.Z., L.M., and W.Z. Visualization: J.C., L.L., X.L., X.W., and X.J. Supervision: S.F., Z.G., and J.-Q.G. Writing—original draft: J.C., X.Z., J.W., and X.J. Writing—review and editing: W.Z., S.F., Z.G., and J.-Q.G. **Competing interests:** J.-Q.G. and J.C. are inventors on one pending patent application related to this work filed by Zhejiang University (China patent no. 202410827214X, filed on 25 June 2024). Z.G. is the cofounder of Zenomics Inc., Zcapsule Inc., and μZen Inc. The other authors declare that they have no competing interests. **Data and materials availability:** All data needed to evaluate the conclusions in the paper are present in the paper and/or the Supplementary Materials.

Submitted 8 August 2024
Accepted 27 February 2025
Published 2 April 2025
10.1126/sciadv.ads3398